Photo-induced electron paramagnetic resonance: A means to identify defects and the defect level throughout the bandgap of ultrawide bandgap semiconductors

Cite as: Appl. Phys. Lett. **124**, 040502 (2024); doi: 10.1063/5.0189934
Submitted: 1 December 2023 · Accepted: 6 January 2024 ·
Published Online: 25 January 2024

M. E. Zvanut,[1,a)] Md Shafiqul Islam Mollik,[1] Mackenzie Siford,[1] and Suman Bhandari[2]

AFFILIATIONS

[1]Department of Physics, University of Alabama at Birmingham, 1720 2nd Ave S., ESH 4100, Birmingham, Alabama 35294, USA
[2]Intel Corporation, 2501 NE Century Blvd., Hillsboro, Oregon 97124, USA

[a)]**Author to whom correspondence should be addressed:** mezvanut@uab.edu

ABSTRACT

Ultrawide bandgap semiconductors (UWBGs) provide great promise for optical devices operating in the near to deep ultraviolet, and recently they have become a viable semiconducting material for high power electronics. From the power grid to electronic vehicles, the intention is to replace massively awkward components with the convenience of a solid state electronic "chip." Unfortunately, the challenges faced by wide bandgap electronic materials, such as GaN and SiC, increase as the bandgap increases. A point defect, for example, can take on more charge states and energy configurations. This perspective describes a method to investigate the many charge states and their associated transitions—photo-induced electron paramagnetic resonance (photo-EPR) spectroscopy. Although not new to the study of defects in semiconductors, photo-EPR studies can probe the entire ultrawide bandgap given the appropriate light source for excitation. Examples provided here cover specific defects in UWBGs, AlN, and Ga_2O_3. The discussion also reminds us how the rapid pace of discovery surrounding this newest class of semiconductors is due, in part, to fundamental research studies of the past, some as far back as a century ago and some based on very different materials systems.

INTRODUCTION TO THE MATERIALS AND POINT DEFECTS

Ultrawide bandgap semiconductors (UWBGs) comprise a relatively new class of materials designed to address the growing need for device-level solutions to high power electronics and ultraviolet (UV) emission and detection. With a bandgap exceeding 5 eV, diamond, gallium oxide (Ga_2O_3), aluminum nitride (AlN), and cubic boron nitride (c-BN) are among the most heavily studied materials of this class. Because of the overwhelming maturity of diamond and the limited advancement of cBN films to date, we leave the significant progress made in the diamond devices and the challenges of c-BN growth to a brief mention at the end. Rather, this perspective focuses on Ga_2O_3 and AlN. Specifically, we describe optical transitions of specific point defects in these materials using photo-induced electron paramagnetic resonance (photo-EPR). While certainly not a benchtop technique, which generates tables of defect configurations and ionization energies, photo-EPR provides a unique approach to optical absorption by monitoring transitions of identifiable defect structures. After a brief description of the materials, this perspective discusses the advantages and challenges of UWBGs and then illustrates the utility of photo-EPR for selected defects in Ga_2O_3 and AlN. In addition to a review of the technique and materials, we remind the reader how fundamental research over the past 100 years has enabled and accelerated the UWBG studies and will likely continue to do so for many different materials in the foreseeable future.

The players

β-Ga_2O_3

Considering the 75+ years of semiconductor history, β-$Ga_2O_3$with a bandgap of ~4.8 eV is a relative newcomer. Flooding the literature about 25 years ago, β-Ga_2O_3 offers controlled *n*-type conduction and a high breakdown field.[1,2] These properties combined with the ability to grow reasonably pure mm-thick material to serve as

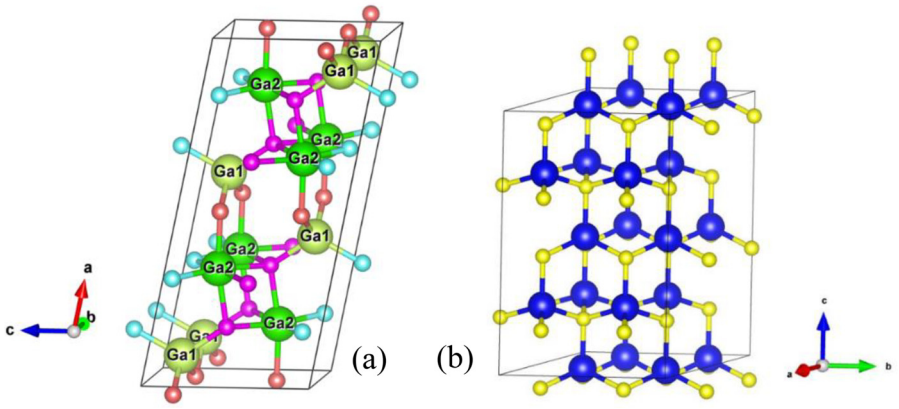

FIG. 1. (a) Monoclinic crystal structure of βGa_2O_3. Ga1 (light green) is tetrahedrally coordinated and Ga2 (dark green) is octahedrally coordinated with O-atoms. O1 (light blue) is bonded to two Ga2 and one Ga1, O2 (brown) to two Ga1 and one Ga2, and O3 (pink) to three Ga2 and one Ga1. (b) Hexagonal structure of AlN. Each Al (blue) is bonded to four N (yellow) and each N, four Al in a distorted tetrahedra.

a substrate for homoepitaxial growth have justified an enormous amount of research.[3] The material may be grown in five different crystal structures, but the monoclinic β phase offers one of the highest bandgaps and is the most thermodynamically stable. Throughout the discussion below, the term Ga_2O_3 will be used exclusively to indicate the β-phase shown in Fig. 1, and most often will refer to crystals grown by the Czochralski (Cz) method.[3] The low symmetry structure offers a rich environment for defect studies. To date, magnetic resonance has identified gallium vacancy centers, along with at least eleven different impurities, the most technologically relevant being Fe.[4,5] In addition, an EPR spectrum characteristic of a neutral donor was identified in Sn-doped and unintentionally doped crystals and is now commonly associated with the Sn or Si dopant.[6] Perhaps the most consequential EPR observation was that of self-trapped hole (STH).[7] The experimental observation of the STH indicates that, as predicted, holes prefer to locate on an oxygen rather than remain in the valence band.[8] Clearly, self-trapping of holes implies that *p*-type conductivity will require an "out-the-box" approach. Nevertheless, prototype devices based on Schottky barrier diodes and field effect transistor structures have been demonstrated.[2]

Hexagonal AlN

The hexagonal crystal structure is shown in Fig. 1(b), where the aluminum is shown as the larger blue circles and the nitrogen as smaller yellow circles. Commonly grown by either physical vapor transport (PVT) or hydride vapor phase epitaxy (HVPE), AlN is a part of the nitride family long recognized for its direct bandgap and consequent emission efficiency in the visible and ultraviolet (UV).[9] Presently, all ranges of the UV spectrum, UV-A, UV-B, and UV-C, may be addressed by AlN wafers, with some limitations. These limitations generally manifest themselves as unwanted absorption in the visible and ultraviolet region of the electromagnetic spectrum due to point defects. For example, as seen in Fig. 2, the transmission is severely compromised as evidenced by the near two-order of magnitude decrease approaching 5 eV. In this particular example, the feature in the spectrum at 2.9 eV has been attributed to various transitions involving the nitrogen and aluminum vacancies.[10,11] Absorption at 4.7 and above 5 eV are sometimes associated with C and V_N, respectively,[12,13] while others attribute an absorption peak near 4 eV to an O_N-V_{Al} complex.[14,15] However, none of these assignments are universally accepted, and there is little confirmation by traditional defect identifying techniques such as magnetic resonance or positron annihilation spectroscopy. Magnetic resonance studies include the optically detected magnetic resonance (ODMR) measurements of Mason *et al.*, as well as EPR identification of the neutral nitrogen vacancy in electron irradiated AlN and the O_N-V_{Al} complex seen in AlN ceramics.[16–18] Of these, the D5 center, originally seen by ODMR, appears to be the most prevalent and is thought to be an isolated oxygen donor, O_N. V_{Al} and V_{Al}-O complexes have also been identified with positron annihilation spectroscopy.[15] Defect identification and crystal purity are essential if AlN is to move beyond an optical material into the world of high power electronics.[19] Recent advances in doping this UWBG semiconductor create a promising future in both optoelectronic and high power devices.[20]

Whether promoting AlN, Ga_2O_3, or any UWBG semiconductor, eliminating the undesired absorption and minimizing the types of trapping/compensating centers are the practical aim of all programs. However, it will be argued here that understanding the source of the absorption or trapping is necessary to achieve these goals. Understanding provides direction for optimizing growth methods and device design, as well as accelerating potential development of future materials.

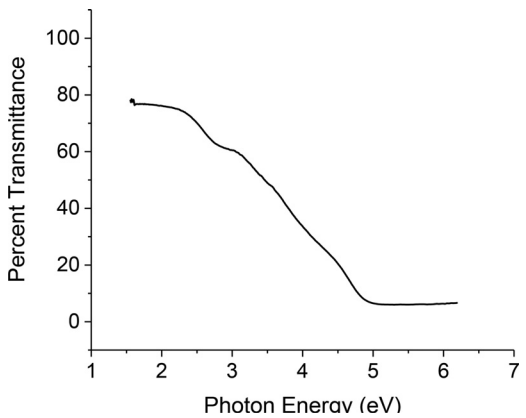

FIG. 2. Transmittance measured on a 0.5 mm thick amber-colored AlN crystal.

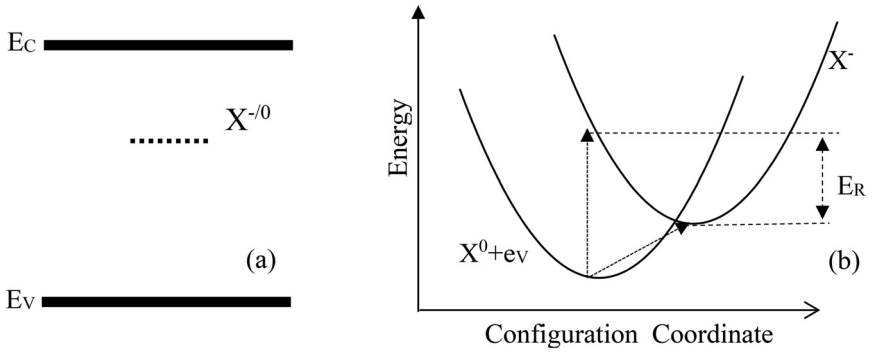

FIG. 3. (a) Schematic of conduction band edge (E_c) and valence band edge (E_v) showing position of hypothetical defect level (dashed line labeled $X^{-/0}$). The vertical axis is electron energy. (b) Hypothetical configuration coordinate diagram of defect X showing the two potential wells: the lower well representing the total energy of the system with X in the neutral state and an electron in the valence band, and the upper well the total system energy with the defect in the negative charge state. The vertical line represents the Franck–Condon transition and the slanted arrow the thermodynamic transition. E_R is the structural relaxation that occurs as the negative charge state relaxes to its equilibrium configuration.

THE FUNDAMENTAL STUDIES OF POINT DEFECTS IN UWBGs

To appreciate the fundamental role and, eventually, the practical role of point defects in electronic or optical materials, one must be introduced to the concept of the defect level or thermodynamic transition level (TTL). Researchers have developed this concept to visualize excitation of electrons or holes from the defect to the band edges and to assist with the understanding of carrier trapping in devices. The two diagrams presented in Fig. 3 illustrate this important concept: (a) for transitions that occur thermally and (b) for those that occur during illumination. In Fig. 3(a), the dashed horizontal line labeled $X^{-/0}$ represents the defect level and may be thought of as the energy required to remove an electron from defect X in its ground state and place it in the conduction band ($X^- => X^0 + e_c$) while allowing the lattice to arrive at a new thermodynamic equilibrium configuration. In this picture, the defect is in the vibrational ground state before and after the transition. For semiconductors with bandgaps ~1 eV or less, most defect transitions may be accessed thermally and the defect level sketch of Fig. 3(a) could be sufficient. For UWBGs, where identification of many defect transitions requires visible or UV illumination, one must consider the configuration coordinate diagram shown in Fig. 3(b). In this idealized drawing, each curve represents the total energy of the system (electronic and vibrational) with the defect in a specific charge state, X^0 for the lower and X^- for the upper. Both the vertical and slanted arrows represent charge transitions. The former (the Frank–Condon transition) is the one most easily detected optically and may be associated with the peak of an absorption spectrum. The second represents the TTL and may be approximated by the threshold of the absorption. As will be highlighted below, such an interpretation can be misleading, and the lattice relaxation, E_R, must be considered. A more detailed discussion of the optical transitions is presented in Ref. 21.

Before discussing point defects further, one should stop and ask "Why spend time on the significance of point defects in semiconductors again? The issues related to semiconductors has been around for more than half a century. What is so special about the UWBG semiconductors?" The answer is straightforward—the ultrawide bandgap creates room for a greater number of charge states of previously identified defects as well as possibilities for different types of defects. For example, the nitrogen vacancy (V_N), a commonly discussed defect in the nitrides, is predicted to have at most one charge transition very close to the valence band edge in InN,[22,23] but 2–3 such transitions may occur throughout the bandgap in the 6 eV bandgap of AlN.[12,18,24–26] These different charge states introduce new sources for trapping as well as electrical compensation. As another example, oxygen substituting for nitrogen (O_N), a common impurity in GaN and AlN, is a simple shallow donor with stable neutral and positive states within the 3.5 eV bandgap of GaN. However, substitutional oxygen becomes a more complex "negative U" or "DX" defect in the wider bandgap AlN.[27,28] The situation is illustrated in Fig. 4 where the slopes of the lines represent the charge state of O_N. Figure 4 shows the formation energy of the + (positive slope), − (negative slope), and neutral (0 slope) charge states of O_N in N-rich AlN and GaN calculated using the density functional theory (DFT). O_N^+ remains the lowest energy charge state of oxygen in GaN until very near the conduction band edge where it transitions to the neutral state. In AlN, on the other hand, at about 5 eV above the valence band edge, the charge state with

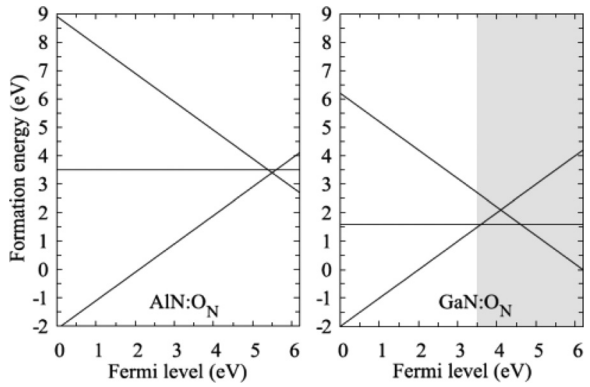

FIG. 4. DFT formation energy calculations for O_N in (a) AlN (bandgap 6 eV) and (b) GaN (bandgap 3.5 eV) for N-rich conditions. In AlN, the horizontal line (neutral state) is never the lowest energy indicating a defect with a negative correlation energy. Reproduced with permission from Gordon *et al.*, Phys. Rev. B **89**, 085204 (2014). Copyright (2014) American Physical Society.

the lowest formation energy switches from positive to negative and the neutral state is never stable. The latter describes the situation for a defect with negative electron correlation energy, where the negative charge state is lower in energy than the neutral state. This creates double trouble as a positively charged defect prefers to trap not one, but two, electrons. In this situation, the traditional effective mass donor is replaced by a deeper, less effective, DX- defect.

Defect levels in many semiconductors have been investigated experimentally and theoretically using a wide range of techniques, some of which were modified to address the greater than 5 eV bandgap. For example, optical excitation replaces the usual thermal stimulation in deep level optical spectroscopy (DLOS), so that a portion of the bandgap larger than that accessible in deep level transient spectroscopy (DLTS) may be probed.[29,30] The results of these measurements may be translated fairly smoothly to practical parameters for device development. Often, however, the nature of the defect is unknown. Identification of the isolated point defects both structurally and chemically relies on techniques such as positron annihilation spectroscopy (PAS) and magnetic resonance.[31–33] Although neither technique may be considered "benchtop characterization," the efforts put forth in the measurement produce an abundance of fruitful fundamental knowledge of the material, knowledge that could be helpful to growers as they tweak temperatures and gas flow rates, and knowledge that might be useful to device engineers as the look for the most effective design. *However, by far the most fruitful use of the knowledge is as a guide to the development of the next generation of materials.*

It is clear that progress in material and/or device development proceeds at a much faster pace than 50 or 100 years ago. Of course, ease of communication and the accelerated rate of data production contribute to this rapid progress, but much may also be attributed to the vast pool of knowledge left to us by those studying fundamental properties decades ago. How is it that a self-trapped hole, a hole which tends to trap onto atoms in the crystal rather than remain in the valence band, was identified in Ga_2O_3 so early in the research? In the 1950s, fundamental studies of alkali halides identified selected defects as V centers in which the removal of an electron from a halide ion may be best viewed as a hole associated with the halide ion rather than a complex involving another point defect such as a vacancy or impurity.[21,34] Armed with the concept, as well as somewhat more powerful computational tools, Varley *et al.* predicted the existence of the center in Ga_2O_3.[8] This was soon followed by the experimental observation of a self-trapped hole by Kananen *et al.* using EPR.[7] Figure 5 shows the defect structure, where the blue lobes represent the p_z orbital of the hole situated on an oxygen in an otherwise perfect crystal. Recognition of the self-trapping property has redirected the search for traditional methods of producing *p*-type Ga_2O_3 since holes apparently tend not to remain in the valence band as necessary for traditional *p*-type conduction. Thus, studies on a completely different materials system, the alkali halides, provided the necessary fuel that then accelerated our understanding of Ga_2O_3 and is guiding the path to *p*-type conductivity.

AN EXAMPLE: DETERMINATION OF A DEFECT LEVEL USING PHOTO-EPR

We will now illustrate the value of fundamental research into point defects using two examples from our own work—identification of a defect and determination of a defect level in ultrawide bandgap semiconductors using photo-EPR. The work highlights how much the

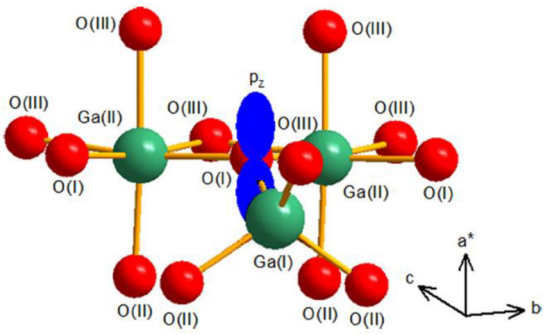

FIG. 5. Model for the self-trapped hole in β-Ga_2O_3. The blue lobes represent the p_z orbital of the oxygen atom on which the hole is trapped. Reproduced with permission from Kananen *et al.*, J. Appl. Phys. **122**, 215703 (2017). Copyright 2017 AIP Publishing LLC.

analysis of defects and optical excitation has benefited from fundamental work reported almost 100 years ago on very different systems. In the first example, photo-EPR is used as a supporting tool to eliminate several possible defect structures. In the second, photo-EPR is applied to a previously identified point defect so that the defect level (TTL) may be determined.

The main strength of magnetic resonance is the formation of a structural and chemical picture of the defects. Basically, the technique is based on the Zeeman effect where the energy of the spin state of an electron may be separated by a magnetic field. Typically, microwaves are used to excite a "spin down" state to a "spin up" state, and appropriate circuitry can detect the spin flip. Technical considerations demand that the spectroscopy consists of sweeping through a range of magnetic fields using a constant microwave frequency. The spin flip is detected when the following condition holds:

$$\mu_B Bg = hf, \tag{1}$$

where μ_B is the Bohr magneton, B is the applied magnetic field at the peak of the microwave absorption, h is Planck's constant, and f is the microwave frequency. "g" is the spectroscopic splitting factor or, simply, "g value," which may be used for initial identification of the defect. One can find numerous reviews and textbooks on the technique. Those pertinent to point defects in crystals include Refs. 32 and 33. Equation (1) represents the simplest situation—the case of a single unpaired (S = 1/2) electron in an isotropic medium. Of the many additional factors contributing to an EPR spectrum, the most pertinent one for this work is the interaction of the "unpaired electron" with the magnetic field caused by the surrounding nuclei with non-zero nuclear spin (I). While this nuclear hyperfine interaction is critical for defect identification, as we will see, it is not always sufficient.

The photo-EPR approach, introduced by Godlewski, is applied here to defects in AlN and Ga_2O_3.[35] A crystal is illuminated with light of selected photon energy, much like an optical absorption measurement. However, in photo-EPR, the sample is placed in a microwave cavity during the illumination, and the amplitude of the magnetic resonance signal is monitored, rather than the transmitted light intensity. The intensity of the EPR signal is proportional to the number of defects in a particular charge state, so changes in the signal at selected wavelengths is interpreted in terms of a change in number of defects in

a particular charge state. Thus, the technique may be used to identify an absorption peak and at least one defect involved in the optical transition. After considerable analysis, the defect level may be determined.

The ultimate power of photo-induced EPR is realized when the interpretation of the EPR spectrum is rigorously confirmed. This is the situation for the example involving Ga_2O_3, where the well-accepted spectrum of neutral Mg substituting for Ga is used to determine the −/0 charge transition level. However, first, we consider a defect in AlN. Unfortunately, the only defect rigorously identified is the neutral nitrogen vacancy, V_N^0, in electron irradiated AlN. Perhaps this is not surprising since the high nuclear spin and atomic abundance of Al and N tend to create broad featureless signals and provide limited spectroscopic information. At least, one signal, however, has sufficient character for reasonable, though not definitive, identification. In this situation, photo-EPR is used to assist with defect identification—eliminating some and introducing other possible candidates. First seen by optically detected magnetic resonance, the EPR signal depicted as the black or red trace in Fig. 6(a) was referred to as D5.[16] As typical of EPR, the spectrum represents the derivative of an absorption because phase sensitive detection is used to increase sensitivity. From the analysis of the EPR spectrum, one knows that the signal is primarily due to the interaction of the paramagnetic electron with one Al. Electron nuclear double resonance studies clarify that the hyperfine observed in EPR involves the one axial Al and identifies three additional hyperfine lines, presumably the basal Al's.[36,37] Significantly, the EPR spectrum reveals no features related to the 100% abundant I = 1 N nearest neighbors. The absence of N hyperfine pointed to a neutral nitrogen vacancy (V_N^0) as an initial suggestion for the defect, but as mentioned, others have convincingly identified a different EPR signal observed after electron irradiation as the V_N^0.[17] With the nitrogen vacancy eliminated as a source of the signal shown in Fig. 6(a), the missing N hyperfine must be reinterpreted as a common impurity with zero nuclear spin, which is substituting for a lattice N. Many suggest oxygen sitting on a nitrogen site (O_N^0) as the logical choice because O easily incorporates into AlN during growth. Preliminary density functional theory (DFT) calculations show that for oxygen sitting on a nitrogen site a significant spin density resides on the axial Al, consistent with the EPR analysis.

Photo-EPR is presently being used to further test the validity of the assignment of the spectrum to a O_N^0. Spectra obtained before illumination (blue), during excitation at 265 nm (black) and subsequent quenching with 730 nm (red), are shown in Fig. 6(a). All were taken at room temperature with the c-axis parallel to the magnetic field. The steady state photo-EPR obtained by monitoring the amplitude of the spectra during illumination is shown in Fig. 6(b). As seen, the signal decreases after exposure to photon energy between 1.5 and 3 eV and increases again from 3.5 eV to above 4.7 eV. The threshold for the decrease and subsequent increase provides a starting point for examining the transition and associated defect level.

A working model for the transition is shown in the inset of Fig. 6(a). Assuming the defect is O_N^0, the first threshold between 1.2 and 1.7 eV could be interpreted as an electron excited from the defect to the conduction band, creating the EPR inactive charge state, O_N^+. Subsequent illumination at about 4 eV re-excites the paramagnetic charge state by exciting an electron from the valence band edge to the defect. The transition levels between various charge states of O_N^0 are calculated by several different groups to be about 1 eV below the conduction band edge,[25,26,28] within a reasonable range of that suggested by the photo-EPR data. Typically, for a donor like O_N, this would be the 0/+ transition. An important distinction here is that the calculated energy, which matches the photo-EPR data most closely is a +/− transition. O_N^0 has a negative correlation energy (negative U), meaning the negative charge state is the lowest energy state and the neutral charge state should be, at most, metastable.

While illumination could excite the neutral state (and thus the EPR spectrum), the spectrum should not be detected prior to illumination. Yet, in one AlN sample with slightly different coloration, the spectrum is present in the dark. Thus, although the thresholds indicated in the photo-EPR are consistent with the O_N^0 assignment, the presence of the defect without illumination suggests that another defect with zero nuclear spin must be responsible. At present, C_N^0 appears to be a reasonable option based on the photo-EPR data. Theory predicts the $C_N^{-/0}$ level to be 1.9–2.0 eV above E_v with no negative U character.[12,38] However, it is not clear whether the substitutional carbon center would produce a significant spin density on the axial Al as indicated by the EPR spectrum. Work, both experimental and computational, is ongoing.

Before proceeding to the second example, it is worth pointing out the relationship between the steady state photo-EPR data and traditional optical absorption where the transmittance through the sample is measured while illuminating with a range of wavelengths. One can think of the first decrease in the photo-EPR data between 2 and 3 eV as corresponding to an absorption curve in a similar energy range. Similarly, the increase starting around 4 eV and peaking at an energy greater than 5 eV would be associated with a traditional absorption peak with threshold at about 4 eV. The significant difference between

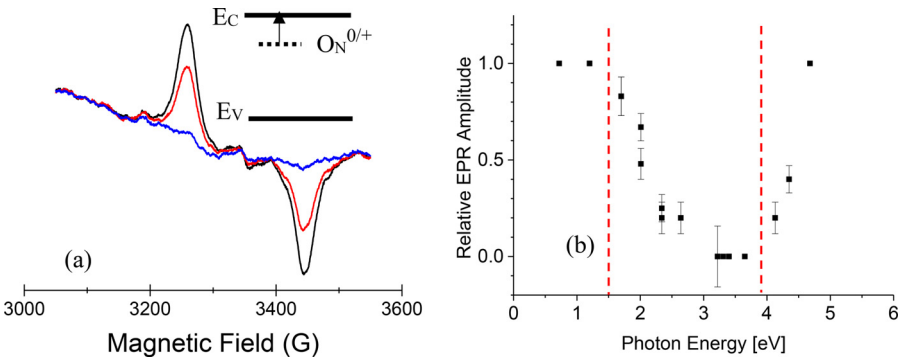

FIG. 6. (a) EPR spectrum in amber-colored AlN obtained with the c-axis parallel to the magnetic field in the dark (blue), during 265 nm illumination (black) and during subsequent 730 nm illumination (red). Inset: Possible transition of the O_N impurity during quenching: $O_N^0 + hf \Rightarrow O_N^+ + e_c$. (b) Steady state photo-EPR data obtained from the sample shown in (a). The dashed vertical lines represent the onset of quenching and excitation.

the measurements is the photo-EPR monitors only a specific defect, while traditional absorption measurements reflects transitions of any and all defects that happen to get excited at a particular energy. For this sample, for instance, the decrease seen in the photo-EPR data likely reflects the commonly observed 2.9 eV absorption and the increase beyond 4 eV, the 5 eV peak. One should be careful, though, not to take the comparison between photo-EPR and transmittance measurements too far. For instance, we never see a "band edge" absorption in photo-EPR since a defect must be involved in the transition, not simply conduction and valence band edges.

In the first example, the steady state photo-EPR measurement is used as an additional tool with which to identify the defect associated with the EPR signal. In our second example, the defect was adequately identified through analysis of the EPR spectrum, and photo-EPR was used to determine the defect level. For this, we monitor the time dependence of the EPR signal intensity to extract the kinetics of the charge transition process. The details of the measurements and analysis may be found in various publications on SiC, GaN, and Ga_2O_3 as well as the original work by Godlewski *et al.*[39–41] Here, we illustrate the effectiveness of the time-dependent photo-EPR method by determining the defect level of Mg in Ga_2O_3.

The time dependence of an EPR spectrum is obtained by monitoring the amplitude of the EPR curve during illumination. In the case of the neutral Mg acceptor, one of the multiple peaks of the spectrum shown in the inset of Fig. 7(a) is chosen. The resulting time-dependent data are shown in Fig. 7(a) for Mg-doped Ga_2O_3 illuminated at 730 nm (black), 660 nm (red), and 590 nm (blue). The change in the number of Mg^0 shown on the y-axis is obtained by comparison of the intensity of the EPR curve to a calibrated standard. The following solution to a first order kinetic equation is fit to the time dependent data,

$$N_{Mg^0_{Ga}}(t) = N_{Mg^0_{Ga}}(0)e^{-t/\tau}, \quad (2)$$

where $N_{Mg^0_{Ga}}(0)$ is the amount of Mg^0_{Ga} at the start of the quenching process and τ is a time constant related to intensity of incident photons (I) and optical cross section (σ) as $\sigma = 1/I\tau$.

Obtaining τ and converting to the optical cross section, the energy dependence of σ may be obtained. Figure 7(b) shows the results for three different samples: floating zone grown (blue triangles) and two pieces of a CZ grown crystal (unfilled triangles and filled stars). The data are similar to that produced by an optical absorption measurement except that all of the points in Fig. 6(b) represent a transition involving Mg^0. In addition to Mg, monitoring other impurities with steady state photo-EPR indicates charge state changes for Fe and Ir above 3 eV (not shown). In this region, Gaussians were fit to the data for the CZ and floating zone crystals. Interestingly, absorption for all samples peaks near 3.3 eV, but the cross section for the FZ sample is different from that of the CZ samples. The difference must be related to the absence of Ir in the FZ samples, but further details cannot be discerned. The data below 3 eV provide much information because participation by other EPR detected defects was not observed. In this region, a modification of an equation developed by Passler is fit to the data.[42] Unlike the Gaussian fits, the equation is based on a well-known model of the electronic cross section coupled with the lattice relaxation, which accompanies the electronic transition. The fit is shown as the red curve in Fig. 7(b) and yields a defect level of 1.2 eV above the valence band edge, along with a lattice relaxation of 1.3 eV. Both agree well with those calculated from DFT.[43,44]

In the spirit of this perspective, it is important to point out how much of the photo-EPR analysis is borrowed from concepts developed in the past for different material systems. For example, the configuration coordinate model shown in Fig. 3, which we have used to evaluate a defect level, is based on the 1920s work of J. Frank and, separately, E. Condon whose main concern was photochemical dissociation and the relative absorption intensities of various molecules.[21,45,46] Several groups studying electronic transitions in semiconductors developed the idea into the form of an optical cross section. Early work borrowed the ideas from nuclear physics to address the electronic cross section.[47] Later, several groups recognized the need to incorporate lattice relaxation and convoluted the electronic and lattice excitations into one transition probability.[42,48,49] Significantly, such ideas need not be limited to situations involving optical excitation. Lattice relaxation has been used to interpret hysteresis seen during electron tunneling in metal insulator semiconductor devices.[50] Thus, the studies, which supply answers to today's problems, were accelerated by ideas developed from completely different materials systems almost a century ago!

LIMITATIONS OF PHOTO-EPR

Of course, no technique is without limitations. The primary concern when interpreting the photo-EPR data is whether the transition observed is a direct defect-to-band transition as seen in the Mg-doped Ga_2O_3 example or an indirect process involving a second defect. Monitoring the time dependence helps sort this out, but still, there are many variables to account for during an optical transition, so one needs to carefully consider several factors: what are the likely intrinsic defects, what other impurities are present, and ultimately, what types

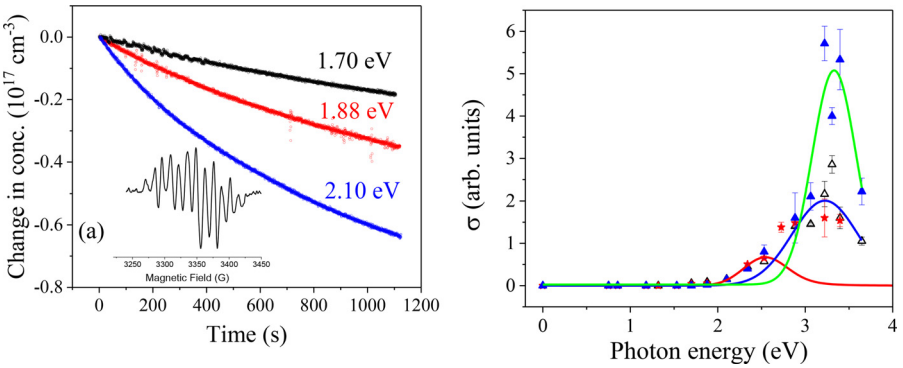

FIG. 7. (a) Time-dependent photo-EPR traces obtained from Ga_2O_3:Mg at different photon energy. INSET: Mg^0_{Ga} EPR spectrum. (b) Cross section obtained from time-dependent photo-EPR data of Ga_2O_3:Mg grown by different methods: floating zone (blue triangles) and two separate pieces of a CZ grown (unfilled triangles and filled stars). The blue and green solid lines are Gaussian fits to the data greater than 3 eV. The red line is obtained from a fit based on a model of Passler[42] using a defect level of 1.2 eV above the valence band edge and lattice relaxation of 1.3 eV.

of transitions and defects are predicted from theory. Fortunately, positron annihilation and sometimes EPR can account for the intrinsic defects, EPR and SIMS may be used to detect impurities, and today, there are a multitude of calculations that provide an excellent guide to interpretation of the photo-EPR spectra.[31,51,52] Nevertheless, even after considering all the other defects as was done in the case of Ga_2O_3:Mg, one must acknowledge that only those transitions with time constants within the resolution of the EPR spectrometer will be detected. Unfortunately, EPR is practically a static technique, with a minimum time resolution of our equipment on the order of 100's of microseconds. Thus, only those charge transfer processes, which can be slowed by the presence of other factors (indeed, defects!) can be detected.[53,54] After detailed analysis, though, one can show that only the magnitude of the cross section, not the energy dependence, is affected by the presence of intermediate transitions.

Another challenge that faces any technique based on magnetic resonance is sensitivity. While EPR is touted for being able to detect defect concentrations as low as 1 ppb, as much as 0.1 cm^3 of material may be required.[32] This is because EPR detects the total number of spins, not concentration, and because the detection limit depends strongly on the linewidth. For a relatively narrow line (~0.1 mT), 10^{12} spins is a typical detection limit,[32] but for lines in Ga_2O_3 and AlN where linewidths are often at least 1 mT, the detection limit increases to 10^{14}. Thus, for a reasonable electronic grade material with defect concentration of 10^{17} cm^{-3}, at least 10^{-3} cm^3 of material is required. The size restriction implies that monolayer films and nanomaterials, which dominate the interest of most semiconductor applications today, are challenging for EPR. In such cases, ODMR and electrically detected magnetic resonance may be successful, particularly for defects involved in spin-sensitive recombination processes. EPR may also be useful when material quantity is limited because the point defects identified through EPR are not unique to the bulk materials in which they are measured. A quick study of SiO_2 films on Si highlights that an enormous amount of knowledge gained about the oxide layer of a MOSFET originated in studies of bulk quartz and high purity silica.[55–57] In particular, radiation damage defects and hydrogen related centers were quickly identified in this critical layer of modern technology due to the detailed studies of its bulk counterpart.[57–60] Surely, the same translation will apply to the Ga_2O_3 and AlN films grown today for future high power or UV sensitive devices.

CLOSING REMARKS

The focus on only two of the prominent UWBGs is not meant to single these out as the most promising or realistic choices for future growth. Nor are these the only ones in which point defects dominate the functionality. Throughout scientific research, diamond has served both as the source and recipient of our fundamental knowledge of point defects in semiconductors. It would take a tome to cover all the studies utilizing concepts from the past, and the reader is directed to the many comprehensive reviews.[61–63] Today, one need only look to single photon emission (SPE) to see how the fundamental studies of diamond have yielded truly new directions of research which has spread to many other semiconductors. The NV center was first identified as a vacancy adjacent to a substitutional nitrogen impurity through the analysis of the EPR signal by Davies.[64] Later optically detected magnetic resonance studies revealed the unique level spacing of the spin system.[65,66] During the ensuing decades, the requirements for SPE evolved and the basic concepts have been used to identify SPE in several other semiconductors.[67–69] The source of the emission in some of these newer systems is being actively investigated, and those responsible for the less-studied emission are yet to be identified. In AlN, in particular, the source of the emission is unclear. The defects presently identified by EPR and, more importantly, ODMR, should provide a rich library of paramagnetic centers, which one might consider as sources of the SPE.

Unlike diamond, investigation into c-BN for electronics is just beginning, largely due to the difficulty growing films with 100% cubic phase. While the production of pure mm-sized crystals may be achieved by high temperature high pressure methods,[70] avoiding incorporation of the many less desirable phases during growth presents a large hurdle to advancement.[71,72] On the other hand, the dopability and band structure predicted from DFT is promising, and a few groups have investigated sulfur and silicon doping.[73,74] Identifying defects in BN and other high nuclear spin materials using EPR is problematic for reasons mentioned earlier in this perspective, but advances can be achieved. ENDOR measurements would likely be beneficial to studies of the EPR active defects in cBN as they have been in AlN. Also, *n*-type doping, when it is realized, is likely to be a fruitful avenue of study for EPR, providing the same insights about transport and dopant stability as has been demonstrated in GaN and AlN. Hopefully, the "lessons learned" from other material systems will be successful in growing functional c-BN films so that the plusses of this UWBGs may eventually be realized.

With the emphasis on EPR, this perspective naturally has focused on bulk material. Crucial to all applications, however, is the layering of one material on top of another forming an interface. Being essentially two-dimensional, the interface is not a natural for EPR studies. Nevertheless, interfacial point defects consisting of dangling bonds are within reach of magnetic resonance if a sufficient amount of interface can be supplied. Studies of the Si dangling bond in the technological giant, the Si/SiO_2 interface, demonstrated the utility of EPR for interfaces. For the future, perhaps studies of the Ga_2O_3/Si or diamond/Ga_2O_3 systems will yield similarly fruitful results.

We end with a reminder that fundamental studies form a strong driving force for advances in material and technology. Clearly, one should not think that they are the only driving force behind the understanding of the materials, nor should one feel that "there is nothing new under the sun." Rather, we want to emphasize how, with time, basic knowledge becomes the facts that feed a generation of new knowledge and, ultimately, new materials and technologies. Considering again the alkali halides, one can reasonably say, that the main contribution of the research in the alkali halides is the research itself because the concepts developed were so successfully applied to many semiconductors, but very little technological advancement based on alkali halides ever emerged. The studies of the alkali halides and other systems have fueled most defect research today and, most likely, will continue to do so well into the future as we tackle new, as yet unrealized UWBGs such as such as the recently predicted rutile GeO_2 and SiO_2, which, by the way, are ideal materials for spin resonance.[75,76]

ACKNOWLEDGMENTS

The author wishes to thank W. B. Fowler for useful conversations and a careful reading of the manuscript. This work was supported as part of the Ultra Materials for a Resilient Energy Grid, an Energy Frontier Research Center funded by the U.S.

Department of Energy, Office of Science, Basic Energy Sciences under Award No. DE-SC0021230 and by the Division of Materials Research at the National Science Foundation, Grant No. 1904325.

The photo-EPR and transmittance measurements and analysis were performed by Mr. Shafiqul Mollik and Ms. Mackenzi Siford, graduate students at UAB, and Dr. Suman Bhandari, presently a staff engineer at Intel.

AUTHOR DECLARATIONS

Conflict of Interest

The authors have no conflicts to disclose.

Author Contributions

Mary E. Zvanut: Conceptualization (equal); Formal analysis (equal); Funding acquisition (equal); Methodology (equal); Project administration (equal); Resources (equal); Supervision (equal); Writing – original draft (equal); Writing – review & editing (equal). **Shafiqul Mollik:** Data curation (supporting); Visualization (supporting). **Mackenzie Siford:** Data curation (supporting). **Suman Bhandari:** Data curation (supporting); Formal analysis (supporting); Methodology (supporting); Visualization (supporting).

DATA AVAILABILITY

The data that support the findings of this study are available from the corresponding author upon reasonable request.

REFERENCES

[1]M. Tadjer, "Toward gallium oxide power electronics," Science **378**, 724–725 (2022).
[2]A. J. Green, J. Speck, G. Xing, P. Moens, F. Allerstam, K. Gumaelius *et al.*, "β-gallium oxide power electronics," APL Mater. **10**, 029201 (2022).
[3]J. Blevins, K. Stevens, A. Lindsey, G. Foundos, and L. Sande, "Development of large diameter semi-insulating gallium oxide (Ga_2O_3) substrates," IEEE Trans. Semicond. Manuf. **32**, 466–472 (2019).
[4]M. L. Meil'man, "EPR of Fe^{3+} ions in β-Ga_2O_3 crystals," Sov. Phys. Solid State **11**, 1403 (1969).
[5]H. J. von Bardeleben, S. Zhou, U. Gerstmann, D. Skachkov, W. R. L. Lambrecht, Q. D. Ho, and P. Deak, "Proton irradiation induced defects in β-Ga_2O_3: A combined EPR and theory study," APL Mater. **7**, 022521 (2019).
[6]M. Yamaga, E. G. Víllora, K. Shimamura, N. Ichinose, and M. Honda, "Donor structure and electric transport mechanism in $\beta-Ga_2O_3$," Phys. Rev. B **68**, 155207 (2003).
[7]B. E. Kananen, N. C. Giles, L. E. Halliburton, G. K. Foundos, K. B. Chang, and K. T. Stevens, "Self-trapped holes in β-Ga_2O_3 crystals," J. Appl. Phys. **122**, 215703 (2017).
[8]J. B. Varley, A. Janotti, C. Franchini, and C. G. Van De Walle, "Role of self-trapping in luminescence and *p*-type conductivity of wide-band-gap oxides," Phys. Rev. **85**, 081109(R) (2012).
[9]R. Sumathi, "Review—Status and challenges in hetero-epitaxial growth approach for large diameter AlN single crystalline substrates," ECS J. Solid State Sci. Technol. **10**, 035001 (2021).
[10]Kawabe, Kazuo, R. H. Tredgold, and Y. Inuishi, "Electrical and optical properties of AlN-a thermostable semiconductor," Electr. Eng. Jpn **87**, 62 (1967).
[11]G. A. Slack, L. J. Schowalter, D. Morellic, and J. A. Freitas, Jr., "Some effects of oxygen impurities on AlN and GaN," J. Cryst. Growth **246**, 287–298 (2002).
[12]A. Alden, J. S. Harris, Z. Bryan, J. N. Baker, P. Reddy, S. Mita *et al.*, "Point-defect nature of the ultraviolet absorption band in AlN," Phys. Rev. Appl. **9**, 054036 (2018).
[13]R. Dalmau, S. Kirby, J. Britt, and R. Schlesser, "Deep level defects in AlN studied by UV-visible spectroscopy," ECS Trans. **109**, 31 (2022).
[14]Q. Yan, A. Janotti, M. Scheffler, and C. G. Van de Walle, "Origins of optical absorption and emission lines in AlN," Appl. Phys. Lett. **105**, 111104 (2014).
[15]J.-M. Maki, I. Makkonen, F. Tuomisto, A. Karjalainen, S. Suihkonen, J. Rais, T. Y. Chemekova, and Y. N. Makarov, "Identification of the V_{Al}-O_N defect complex in AlN single crystals," Phys. Rev. B **84**, 081204(R) (2011).
[16]P. M. Mason, H. Przybylinska, G. D. Watkins, W. J. Choyke, and G. A. Slack, "Optically detected electron paramagnetic resonance of AlN single crystals," Phys. Rev. B **59**, 1937 (1999).
[17]N. T. Son, A. Gali, Á. Szabó, M. Bickermann, T. Ohshima, J. Isoya, and E. Janzén, "Defects at nitrogen site in electron-irradiated AlN," Appl. Phys. Lett. **98**, 242116 (2011).
[18]S. Schweizer, U. Rogulis, J.-M. Spaeth, L. Trinkler, and B. Berzina, "Investigation of oxygen-related luminescence centres in AlN ceramics," Phys. Status Solidi B **219**, 171 (2000).
[19]A. L. Hickman, R. Chaudhuri, S. J. Bader, K. Nomoto, L. Li, J. C. M. Hwang, H. Grace Xing, and D. Jena, "Next generation electronics on the ultrawide-bandgap aluminum nitride platform," Semicond. Sci. Technol. **36**, 044001 (2021).
[20]W. A. Doolittle, C. M. Matthews, H. Ahmad, K. Motoki, S. Lee, A. Ghosh *et al.*, "Prospectives for AlN electronics and optoelectronics and the important role of alternative synthesis," Appl. Phys. Lett. **123**, 070501 (2023).
[21]W. Beall Fowler, *The Physics of Color Centers* (Academic Press, New York and London, 1968).
[22]C. Stampfl, C. G. Van de Walle, D. Vogel, P. Krüger, and J. Pollmann, "Native defects and impurities in InN: First-principles studies using the local-density approximation and self-interaction and relaxation-corrected pseudopotentials," Phys. Rev. B **61**, R7846 (2000).
[23]T. L. Tansley and R. J. Egan, "Point-defect energies in the nitrides of aluminum, gallium, and indium," Phys. Rev. B **45**, 10942 (1992).
[24]B. Szucs, A. Gali, Z. Hajnal, P. Deak, and C. G. Van de Walle, "Physics and chemistry of hydrogen in the vacancies of semiconductors," Phys. Rev. B **68**, 085202 (2003).
[25]C. Kai, H. Zang, J. Ben, K. Jiang, Z. Shi, Y. Jia, X. Cao, W. Lü, X. Sun, and D. Li, "Origination and evolution of point defects in AlN film annealed at high temperature," J. Lumin. **235**, 118032 (2021).
[26]Y. Chen, L. Wu, D. Liang, P. Lu, J. Wang, J. Chen, H. Cao, and L. Han, "Investigation of native defects and impurities in X-N (X = Al, Ga, In)," Comput. Mater. Sci. **188**, 110169 (2021).
[27]M. D. McCluskey, C. G. Van de Walle, N. M. Johnson, D. P. Bour, and M. Kneissl, "DX centers in AlGaN," Int. J. Mod. Phys. B **13**, 1363 (1999).
[28]L. Gordon, J. L. Lyons, A. Janotti, and C. G. Van de Walle, "Hybrid functional calculations of DX centers in AlN and GaN," Phys. Rev. B **89**, 085204 (2014).
[29]A. Chantre, G. Vincent, and D. Bois, "Deep-level optical spectroscopy in GaAs," Phys. Rev. B **23**, 5335 (1981).
[30]E. Farzana, E. Ahmadi, J. S. Speck, A. R. Arehart, and S. A. Ringel, "Deep level defects in Ge-doped (010) β-Ga_2O_3 layers grown by plasma-assisted molecular beam epitaxy," J. Appl. Phys. **123**, 161410 (2018).
[31]F. Tuomisto, "Identification of point defects in multielement compounds and alloys with positron annihilation spectroscopy: Challenges and opportunities," Phys. Status Solidi RRL **15**, 2100177 (2021).
[32]J. A. Weil, J. R. Bolton, and J. E. Wertz, *Electron Paramagnetic Resonance* (John Wiley & Sons, Inc, New York, 1994).
[33]A. Abragam and B. Bleaney, *Electron Paramagnetic Resonance of Transition Ions* (Dover Publications, New York, 1986).
[34]T. G. Castner and W. Kanzig, "The electronic structure of V-centers," J. Phys. Chem. Solids **3**, 178 (1957).
[35]M. Godlewski, "On the application of the Photo-EPR technique to the studies of photoionization, DAP recombination, and non-radiative recombination processes," Phys. Status Solidi A **90**, 11 (1985).
[36]V. A. Soltamov, I. V. Ilyin, A. A. Soltamova, E. N. Mokhov, and P. G. Baranov, "Identification of the deep level defects in AlN single crystals by electron paramagnetic resonance," J. Appl. Phys. **107**, 113515 (2010).
[37]S. M. Evans, N. C. Giles, L. E. Halliburton, G. A. Slack, S. B. Schujman, and L. J. Schowalter, "Electron paramagnetic resonance of a donor in aluminum nitride crystals," Appl. Phys. Lett. **88**, 62112 (2006).
[38]J. L. Lyons, A. Janotti, and C. G. Van de Walle, "Effects of carbon on the electrical and optical properties of InN, GaN, and AlN," Phys. Rev. B **89**, 035204 (2014).

[39]S. Bhandari, J. L. Lyons, D. Wickramaratne, and M. E. Zvanut, "Optical transitions of neutral Mg in Mg-doped β-Ga_2O_3," APL Mater. **10**, 021103 (2022).
[40]M. Godlewski, "Photoelectron paramagnetic resonance studies of ionization transitions of chromium impurities in ZnS and GaAs," J. Appl. Phys. **56**, 2901 (1984).
[41]N. T. Son, B. Magnusson, and E. Janzén, "Photoexcitation-electron-paramagnetic-resonance studies of the carbon vacancy in 4H-SiC," Appl. Phys. Lett. **81**, 3945–3947 (2002).
[42]R. Pässler, "Alternative electronic parts for multiphonon-broadened photoionization cross sections of deep levels in SiC," J. Appl. Phys. **97**, 113533 (2005).
[43]J. L. Lyons, "A survey of acceptor dopants for β-Ga_2O_3," Semicond. Sci. Technol. **33**, 05LT02 (2018).
[44]Q. Duy Ho, T. Frauenheim, and P. Deák, "Theoretical confirmation of the polaron model for the Mg acceptor in β-Ga_2O_3," J. Appl. Phys. **124**, 145702 (2018).
[45]E. Condon, "A theory of intensity distribution in band systems," Phys. Rev. **28**, 1182 (1926).
[46]E. U. Condon, "The Franck-Condon principle and related topics," Am. J. Phys. **15**, 365 (1947).
[47]G. Lucovsky, Solid State Commun. **3**, 299 (1965).
[48]A. A. Kopylov and A. N. Pikhtin, "Effect of temperature on the optical-absorption spectra of deep centers in semiconductors," Sov. Phys. Solid State **16**, 1200 (1975).
[49]D. Lang and R. Logan, "Large-lattice-relaxation model for persistent photoconductivity in compound semiconductors," Phys. Rev. Lett. **39**, 635 (1977).
[50]W. B. Fowler, J. K. Rudra, M. E. Zvanut, and F. J. Feigl, "Hysteresis and Franck-Condon relaxation in insulator-semiconductor tunneling," Phys. Rev. B **41**, 8313 (1990).
[51]G. D. Watkins and L. M. Slifkin, in *Point Defects in Solids: Semiconductors and Molecular Crystals*, edited by J. H. Crawford (Springer US, Boston, MA, 1975), Vol. 2, pp. 333–392.
[52]J. L. Lyons and C. G. Van de Walle, "Computationally predicted energies and properties of defects in GaN," npj Comput. Mater. **3**, 12 (2017).
[53]S. Bhandari, "Optical absorption of point defects in doped gallium oxide determined by photo-induced electron paramagnetic resonance spectroscopy," Ph. D. dissertation (The University of Alabama at Birmingham, Birmingham, AL, 2022).
[54]S. Paudel, "Defect properties determined by photo-induced electron paramagnetic resonance spectroscopy in carbon-doped gallium nitride substrates," Ph. D. dissertation (The University of Alabama at Birmingham, Birmingham, AL, 2022).
[55]D. L. Griscom, "Optical properties and structure of defects in silica glass," J. Ceram. Soc. Jpn. **99**, 923–942 (1991).
[56]D. L. Griscom, "Electron spin resonance in glasses," J. Non-Cryst. Solids **40**, 211–272 (1980).
[57]J. A. Weil, "A review of the EPR spectroscopy of the point defects in α-quartz: The decade 1982–1992," in *Physics and Chemistry of SiO2 and the Si-SiO2 Interface 2* (Springer Nature, 1993), pp. 131–144.
[58]D. L. Griscom and E. J. Friebele, "Effects of ionizing radiation on amorphous insulators," Radiat. Effects **65**(1–4), 63–72 (1982).
[59]S. J. Moxim, J. P. Ashton, P. M. Lenahan, M. E. Flatté, N. J. Harmon, and S. W. King, "Observation of radiation-induced leakage current defects in MOS oxides with multifrequency electrically detected magnetic resonance and near-zero-field magnetoresistance," IEEE Trans. Nucl. Sci. **67**, 228–233 (2020).
[60]M. E. Zvanut, T. L. Chen, R. E. Stahlbush, E. S. Steigerwalt, and G. A. Brown, "Generation of thermally induced defects in buried SiO_2 films," J. Appl. Phys. **77**, 4329 (1995).
[61]J. H. N. Loubser and J. A. Van Wyk, "Electron spin resonance in the study of diamond," Rep. Prog. Phys. **41**, 1201 (1978).
[62]D. J. Twitchen, D. C. Hunt, M. E. Newton, J. M. Baker, T. R. Anthony, and W. F. Banholzer, "Electron paramagnetic resonance (EPR) and optical absorption studies of defects created in diamond by electron irradiation damage at 100 and 350 K," Physica B **273–274**, 628–631 (1999).
[63]A. M. Edmonds, M. E. Newton, P. M. Martineau, D. J. Twitchen, and S. D. Williams, "Electron paramagnetic resonance studies of silicon-related defects in diamond," Phys. Rev. B **77**, 245205 (2008).
[64]J. H. N. Loubser and J. A. van Wyk, "Optical spin polarization in a triplet state in irradiated and annealed type Ib diamonds," Diam. Res. **9**, 11 (1977).
[65]G. Davies and M. F. Hamer, "Optical studies of the1.945eV vibronic band in diamond" Proc. R. Soc. London, Ser. A **348**, 285 (1967).
[66]E. van Oort, N. B. Manson, and M. Glasbeek, "Optically detected spin coherence of the diamond N-V centre in its triplet ground state," J. Phys. C: Solid State Phys. **21**, 4385 (1988).
[67]S. Gupta, W. Wu, S. Huang, and B. I. Yakobson, "Single-photon emission from two-dimensional materials, to a brighter future," J. Phys. Chem. Lett. **14**, 3274–3284 (2023).
[68]M. Etzelmüller Bathen and L. Vines, "Manipulating single-photon emission from point defects in diamond and silicon carbide," Adv. Quantum Technol. **4**, 2100003 (2021).
[69]Y. Xue, H. Wang, N. Xie, Q. Yang, F. Xu, B. Shen, J-j Shi, D. Jiang, X. Dou, T. Yu, and B-q Sun, "Single-photon emission from point defects in aluminum nitride films," J. Phys. Chem. Lett. **11**, 2689–2694 (2020).
[70]T. Taniguchi, T. Teraji, S. Koizumi, K. Watanabe, and S. Yamaoka, "Appearance of n-type semiconducting properties of cBN single crystals grown at high pressure," Jpn. J. Appl. Phys., Part 2 **41**, L109–L 111 (2002).
[71]J. M. Brown, S. Vishwakarma, D. J. Smith, and R. J. Nemanich, "Nucleation of cubic boron nitride on boron-doped diamond via plasma enhanced chemical vapor deposition," J. Appl. Phys. **133**, 215303 (2023).
[72]X. W. Zhang, "Doping and electrical properties of cubic boron nitride thin films: A critical review," Thin Solid Films **544**, 2–12 (2013).
[73]H. Yina, H.-G. Boyen, P. Ziemann, B. Dohuard, L. Houssiau, F. Renaux, M. Hecq, and C. Bittencourt, "Purity of epitaxial cubic boron nitride films on (001) diamond—A prerequisite for their doping," Diamond Relat. Mater. **17**, 276–282 (2008).
[74]C. Ronning, A. D. Banks, B. L. McCarson, R. Schlesser, Z. Sitar, R. F. Davis, B. L. Ward, and R. J. Nemanich, "Structural and electronic properties of boron nitride thin films containing silicon," J. Appl. Phys. **84**, 5046 (1998).
[75]H. Takane and K. Kaneko, "Establishment of a growth route of crystallized rutile GeO_2 thin film ($\geq$1 μm/h) and its structural properties," Appl. Phys. Lett. **119**, 062104 (2021).
[76]J. L. Lyons and A. Janotti, "A *p*-type dopable ultrawide-bandgap oxide," J. Phys: Condens. Matter **36**, 085501 (2023).